ACS OMEGA

Open Access

http://pubs.acs.org/journal/acsodf

Article

Preparation of the N, P-Codoped Carbonized UiO-66 Nanocomposite and Its Application in Supercapacitors

Chunyan Wang,[§] Jingwei Su,[§] Haiyan Lan, Chongshi Wang, Yi Zeng, Rong Chen,* and Tianxiang Jin*

Cite This: *ACS Omega* 2023, 8, 44689−44697

Read Online

ACCESS | Metrics & More | Article Recommendations

ABSTRACT: Preparing high-performance electrode materials from metal−organic framework precursors is currently a hot research topic in the field of energy storage materials. Improving the conductivity of such electrode materials and further increasing their specific capacitance are key issues that must be addressed. In this work, we prepared phosphoric acid-functionalized UiO-66 material as a precursor for carbonization, and after carbonization, it was combined with activated carbon to obtain nitrogen-/phosphorus-codoped carbonized UiO-66 composite material (N/P-C-UiO-66@AC). This material exhibits excellent conductivity. In addition, the carbonized product ZrO_2 and the nitrogen-/phosphorus-codoped structure evidently improve the pseudocapacitance of the material. Electrochemical test results show that the material has a good electrochemical performance. The specific capacitance of the supercapacitor made from this material at 1.0 A/g is 140 F/g. After 5000 charge−discharge cycles at 10 A/g, its specific capacitance still remains at 88.5%, indicating that the composite material has good cycling stability. The symmetric supercapacitor assembled with this electrode material also has a high energy density of 11.0 W h/kg and a power density of 600 W/kg.

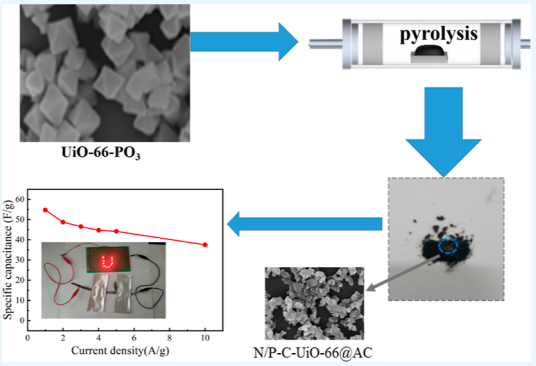

1. INTRODUCTION

Supercapacitors (SCs) have attracted much attention due to their advantages such as fast charge and discharge rates, high power density, and long service life.[1] However, the energy density of SCs is generally low,[2] which significantly limits their applications in the field of energy storage. To solve this problem, it is crucial to develop electrode materials with a high energy density that can be used for SCs.

Doping with heteroatoms is a common method to improve the energy density of carbon-based SCs. Doped carbon materials refer to carbon materials where noncarbon elements such as nitrogen, oxygen, phosphorus, sulfur, selenium, and others are covalently bonded to the carbon skeleton. Since doped elements differ from carbon in terms of electronegativity and the chemical structure they form, doping significantly affects the electronic cloud distribution state of the carbon skeleton structure, thus affecting the physicochemical properties of carbon materials.[3] Nitrogen doping is an effective means to improve the electrochemical performance of activated carbon (AC). First, nitrogen-containing groups can undergo reversible redox reactions during charge and discharge processes, providing a certain amount of pseudocapacitance. Second, the electronic configuration of nitrogen atoms contains a pair of lone electrons, which can change the electronic configuration of carbon atoms when doped into the carbon lattice, leading to a shift in the Fermi level of the carbon material's valence band, thereby increasing the electron conductivity of the carbon material. In addition, due to the relatively high electronegativity of nitrogen, it can also improve the wettability of the carbon material surface, increasing its affinity to aqueous electrolytes.[4,5] Li[6] et al. have prepared nitrogen-doped AC fibers by spinning a mixture of polyethylenimine and ethylene tar pitch, followed by carbonization and activation. Their specific capacitance can reach 314 F g^{-1} (0.5 A g^{-1}), which is a 62% increase compared with that of undoped materials. In addition, phosphorus doping can also increase the pseudocapacitance of carbon materials and expand the operating voltage range of SCs in aqueous electrolyte environments, thereby improving their energy density.[7]

Therefore, codoping nitrogen and phosphorus into the carbon material matrix to prepare N, P-codoped carbon materials is expected to effectively improve the energy density of SCs.[8]

Metal−organic frameworks (MOFs) are typical porous coordination materials formed by the self-assembly of metal ions or clusters with organic ligands through coordination

Received: July 27, 2023
Accepted: September 26, 2023
Published: November 16, 2023

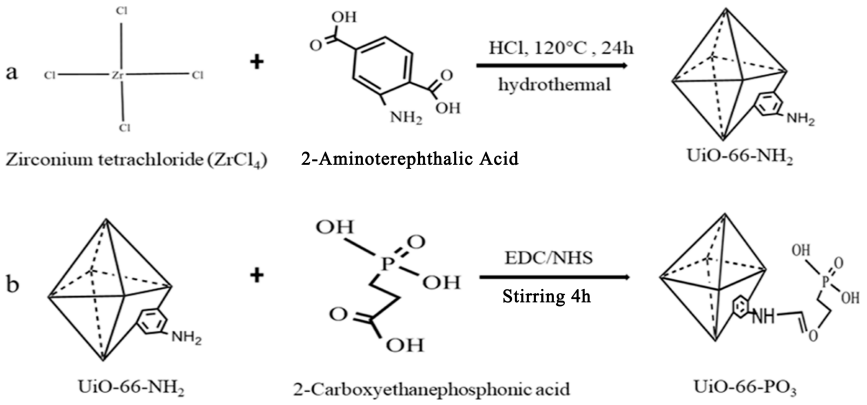

Figure 1. Synthesis procedure of UiO-66-NH_2 (a) and UiO-66-PO_3 (b).

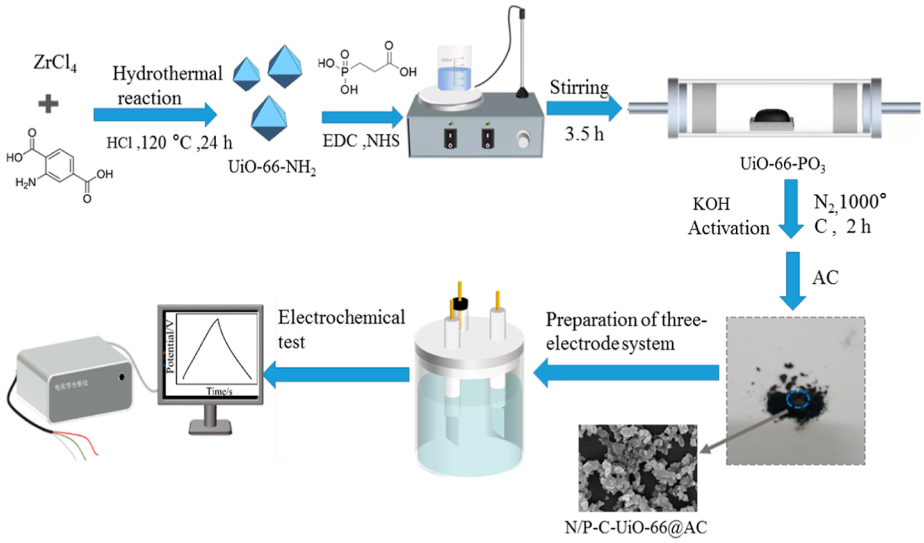

Figure 2. chematic diagram of the preparation and analysis testing of N/P-C-UiO-66@AC composites.

bonds.[9−12] Among them, UiO-66 (Zr-MOF) is suitable as a precursor for nitrogen-doped AC due to its high unsaturation and nitrogen content.[13] In addition, UiO-66 contains a large number of amino groups, which endow it with high chemical reactivity. Therefore, phosphorus-containing groups can be introduced into UiO-66 through chemical reactions, and this modified UiO-66 can be used as a precursor for carbonization to prepare N, P-codoped AC materials.[14,15]

However, carbonized MOF-based electrodes have poor electrical conductivity due to the apparent granularity of the MOF-derived materials, hindering the continuous transport of electrons.[16,17]

For this issue, carbonized MOF can be combined with materials that have good conductivity to improve its electrical conductivity, thereby improving its electrochemical performance and energy storage capacity.[18,19] In this work, carbonized UiO-66-NH_2 (cUiO-66) was mixed with highly conductive AC to further enhance the electrical conductivity of this material (N-C-UiO-66@AC). In addition, in order to dope the carbonized material with both N and P elements simultaneously, P atoms were introduced into the precursor (UiO-66-NH_2) before carbonization through chemical reactions, producing nitrogen−phosphorus-codoped carbonized UiO-66 composite (N/P-C-UiO-66@AC). Compared with N-C-UiO-66@AC, the N/P-C-UiO-66@AC composite material prepared by this method has excellent electrochemical properties. Electrochemical testing revealed that the specific capacitance of the composite material at 1.0 A/g was 140 F/g, and after 5000 cycles of charge and discharge at 10 A/g, its specific capacitance retention rate was 88.5%, indicating excellent cycling stability of this composite material.

2. EXPERIMENTAL SECTION

2.1. Preparation of Materials. *2.1.1. Synthesis of UiO-66-NH_2.* 2.7 mmol (0.63 g) of $ZrCl_4$ and 3.78 mmol (0.69 g) of 2-aminoterephthalic acid were added into a beaker and mixed with 42 mL of dimethylformamide (DMF). The mixture was stirred until the solid dissolved, and then 10 mL of concentrated hydrochloric acid was added and stirred for 30 min. The reaction mixture was then transferred to a PTFE-lined autoclave and reacted at 120 °C for 24 h. After completion of the reaction, the product was centrifuged and washed three times with DMF and methanol. The resulting solid was dried at 60 °C for 12 h to obtain UiO-66-NH_2.

2.1.2. Synthesis of UiO-66-PO_3. 0.26 g amount of 3-phosphonopropionic acid was added to 20 mL of 2-morpholinoethanesulfonic acid buffer solution. Then, 0.65 g of EDC and 0.39 g of NHS were added to activate the carboxylic acid groups and stirred for 30 min. Afterward, 0.5 g of UiO-66-NH_2 was added and stirred for another 3 h. After completion of the reaction, the solid was centrifuged and

https://doi.org/10.1021/acsomega.3c05500
ACS Omega 2023, 8, 44689−44697

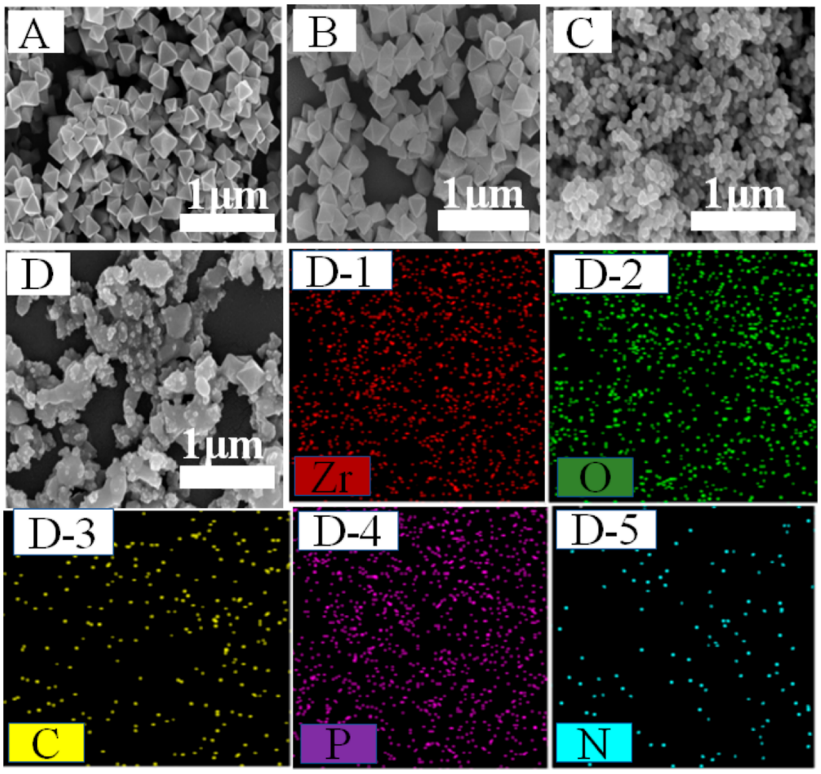

Figure 3. SEM maps of (A) UiO-66-NH_2, (B) UiO-66-PO_3, (C) N-C-UiO-66, and (D) N/P-C-UiO-66 and elemental mapping of (D-1) Zr, (D-2) O, (D-3) C, (D-4) P, and (D-5) N.

washed five times with deionized water (DI). The resulting solid was dried at 60 °C for 12 h to obtain UiO-66-PO_3. Figure 1a,b shows the synthesis steps of UiO-66-NH_2 and UiO-66-PO_3, respectively.

2.1.3. Preparation of N-C-UiO-66 and N/P-C-UiO-66. UiO-66-NH_2 and UiO-66-PO_3 prepared as described above were separately placed in a tube furnace. Under a N_2 atmosphere, the temperature was ramped up to 1000 °C at a rate of 5 °C/min, then held at 1000 °C for 2 h, and finally cooled down to room temperature at the same rate. The resulting products were washed with hydrochloric acid to remove impurities, followed by rinsing with DI. The products were then dried in a vacuum drying oven at 70 °C to obtain N-C-UiO-66 and N/P-C-UiO-66, respectively.

2.1.4. Preparation of N-C-UiO-66@AC and N/P-C-UiO-66@AC Composite Materials. N-C-UiO-66 and N/P-C-UiO-66 were mixed with AC at a mass ratio of 10:1 to obtain the products N-C-UiO-66@AC and N/P-C-UiO-66@AC composite materials. The preparation of N/P-C-UiO-66@AC and the electrochemical test of the electrode prepared from it are shown in Figure 2.

2.1.5. Assembly of the N/P-C-UiO-66@AC//N/P-C-UiO-66@AC Supercapacitor. To prepare the two-electrode cell, we solvated the N/P-C-UiO-66@AC electrodes with KOH electrolytes and placed them on nickel foam. They were then compressed using a hydraulic press, applying a pressure of 10 MPa for 30 s to form well-adhered films on the nickel foam. To create a symmetric SC, two identical N/P-C-UiO-66@AC samples on separate nickel foam were used as electrodes with no additional additives. They were separated by a TF4535 fiber membrane soaked with electrolytes. All components were assembled into a layered structure and tightly sealed with an aluminum plastic film for electrochemical measurements. DI with high-purity standards was used in this work.

2.2. Materials Characterization. Feld emission scanning electron microscopy (FESEM) was performed on a Nova Nano SEM 450 scanning electron microscope. X-ray photoelectron spectroscopy (XPS) was used to analyze the composition and chemical state of the surface elements and functional groups. The crystal structure of the sample was studied by XRD (D8 ADVANCE, Bruker, Germany).

2.3. Electrochemical Tests. The electrochemical tests were conducted by using a CHI660E workstation (Shanghai Chenhua) in a 3 M KOH aqueous solution. To investigate the electrochemical performance of the samples, a three-electrode system was employed. The reference electrode was a saturated calomel electrode, and Pt wire served as the counter electrode. The specific capacitances (C_s) of the individual electrode and the two-electrode cell were determined by analyzing the galvanostatic discharge curves using eq 1. Furthermore, the specific energy density (E_c) and specific power density (P_c) were calculated based on eqs 2 and3, respectively

$$C_s = \frac{I\Delta t}{m\Delta U} \tag{1}$$

$$E_c = \frac{C_s \Delta U^2}{2 \times 3.6} \tag{2}$$

$$P_c = \frac{E_c \times 3600}{\Delta t} \tag{3}$$

where I represents the discharge current, Δt denotes the discharge time, and m represents the mass of the active material in the three-electrode system. In the case of the two-

https://doi.org/10.1021/acsomega.3c05500
ACS Omega 2023, 8, 44689−44697

electrode cell, m refers to the total active mass of both electrodes. Additionally, ΔU represents the voltage window.

3. RESULTS AND DISCUSSION

3.1. Characterization of the Materials. Figure 3A,B shows the SEM images of UiO-66-NH_2 and UiO-66-PO_3, respectively. As seen, both UiO-66-NH_2 and UiO-66-PO_3 exhibit regular octahedral shapes. This result indicates that the structure of UiO-66-PO_3 was not destroyed after phosphonation. However, the surface of UiO-66-PO_3 looks rougher than that of UiO-66-NH_2, which suggests that the phosphonation process produced many defects in the interior of UiO-66-PO_3. N-C-UiO-66 and N/P-C-UiO-66 were obtained after high-temperature calcination at 1000 °C. As shown in Figure 3C,D, the morphologies of N-C-UiO-66 and N/P-C-UiO-66 changed significantly from an octahedral shape to an irregular shape. Additionally, their particle size decreased significantly compared to that before carbonization. This phenomenon suggests that the octahedral framework of UiO-66 collapsed and twisted during carbonization, which may provide more redox-active sites.

In addition to the above analysis, energy-dispersive spectrometry (EDS) was used in combination with SEM to study the types and contents of elements in the material. The element mapping results for Zr, O, C, P, and N in the N/P-C-UiO-66@AC composite material are shown in Figure 3D-1, D-2, D-3, D-4, and D-5, respectively. These figures indicate that the five elements are evenly distributed in the material. These results demonstrate that the composite material contains Zr, O, C, P, and N, indicating successful doping of N and P elements into the material.

In order to study the changes in the crystal structure and morphology of the composite materials before and after modification and carbonization, XRD characterization was carried out on UiO-66-NH_2, UiO-66-PO_3, and N/P-C-UiO-66@AC. The test results are shown in Figure 4. It can be seen

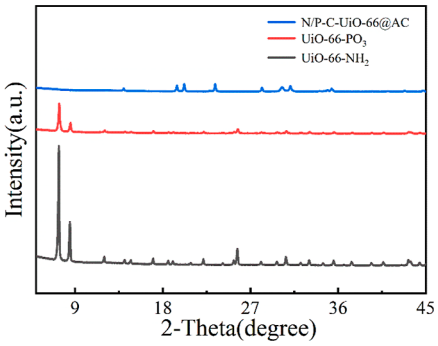

Figure 4. XRD patterns of UiO-66-NH_2, UiO-66-PO_3, and N/P-C-UiO-66@AC.

from the figure that the position, height, and width of the diffraction peaks of UiO-66-NH_2 are consistent with those reported in previous literature,[20] indicating the successful preparation of UiO-66-NH_2. The intensity of the diffraction peak at the same position of UiO-66-PO_3 after modification is weaker than that of UiO-66-NH_2, indicating that defects were generated inside the phosphorized UiO-66-NH_2 after phosphonation, but the crystal structure remains basically unchanged.[21] After high-temperature carbonization, the characteristic peak of UiO-66-NH_2 in N/P-C-UiO-66@AC disappeared, indicating that the crystal structure changed and partially collapsed from the original regular octahedral structure to an amorphous state, which is consistent with the SEM results in Figure 3.

To further investigate the chemical structure of the material, XPS was used to study the elemental composition and valence state of N/P-C-UiO-66@AC. As shown in Figure 5A, the XPS spectra of UiO-66-NH_2, N-C-UiO-66@AC, and N/P-C-UiO-66@AC reveal that the synthesized composite material contains five elements, including P, Zr, C, N, and O. The P 2p peak in the N/P-C-UiO-66@AC spectrum indicates the successful doping of P in the UiO-66 substrate using the experimental method in this work. Subsequently, the high-resolution XPS spectra of Zr 3d were studied to analyze the oxidation state of Zr (Figure 5B). Two characteristic peaks at 185.6 and 183.2 eV, representing Zr $3d_{5/2}$ and Zr $3d_{3/2}$, respectively, were observed in both the N-C-UiO-66@AC and N/P-C-UiO-66@AC spectra. The splitting width of Zr 3d was 2.4 eV, indicating the presence of the Zr^{4+} valence state.[22] Figure 5C shows the high-resolution XPS spectra of the O 1s peak. The two characteristic peaks at 531.1 and 532.5 eV demonstrate the existence of PO^{3-} and O−Zr−O,[23] which is consistent with the previous analysis of the Zr 3d high-resolution XPS spectra and indicates the presence of ZrO_2 in the composite material. Figure 5D shows the high-resolution XPS spectra of C 1s, where three peaks at 285.5, 286.8, and 289.9 eV are attributed to the characteristic peaks of C−Zr, C−N, and O−C═O, respectively. Figure 5E shows the high-resolution XPS spectra of N 1s, which can be divided into two peaks at around 400.4 and 402.7 eV, corresponding to pyrrolic N and quaternary N in the composite material, respectively.[24] Moreover, there is a clear peak at 133.5 eV in the P 2p spectrum (Figure 5F), which combined with the previous high-resolution O 1s spectra confirms the presence of P as PO^{3-} with a valence state of +5. These results indicate the successful doping of the N and P elements in the composite material.

3.2. Electrochemical Properties Analysis. To investigate electrochemical properties, N-C-UiO-66@AC and N/P-C-UiO-66@AC were tested as working electrodes in a three-electrode system in an electrolytic cell containing 6 M KOH. Figure 6A shows the Nyquist plots of the UiO-66-NH_2, UiO-66-PO_3, N-C-UiO-66@AC, and N/P-C-UiO-66@AC electrodes, where the intercept of the curves on the x-axis represents the equivalent series resistance (R_s), the diameter of the high-frequency semicircle represents the charge transfer resistance (R_{ct}), and the slope of the line in the low-frequency region is related to the ion diffusion process.[25−28] The R_s values of N-C-UiO-66@AC and N/P-C-UiO-66@AC were evidently lower than those of UiO-66-NH_2 and UiO-66-PO_3, indicating that the carbonization of MOF materials and the introduction of AC have significantly improved the conductivity of the materials. The R_s values of UiO-66@AC and N/P-C-UiO-66@AC electrodes were 0.766 and 0.769 Ω, respectively, indicating that P doping did not significantly decrease the conductivity of the material. The slope of N/P-C-UiO-66@AC is significantly larger than that of N-C-UiO-66@AC, indicating that its ion diffusion rate is faster.[29] This should be attributed to the introduction of the P element, which maintains the original porous structure of UiO-66 and increases the hydrophilicity of N-C-UiO-66.

The galvanostatic charge−discharge (GCD) curves of these four samples measured at a current density of 1.0 A/g are shown in Figure 6B. It can be seen from the figure that all of

https://doi.org/10.1021/acsomega.3c05500
ACS Omega 2023, 8, 44689−44697

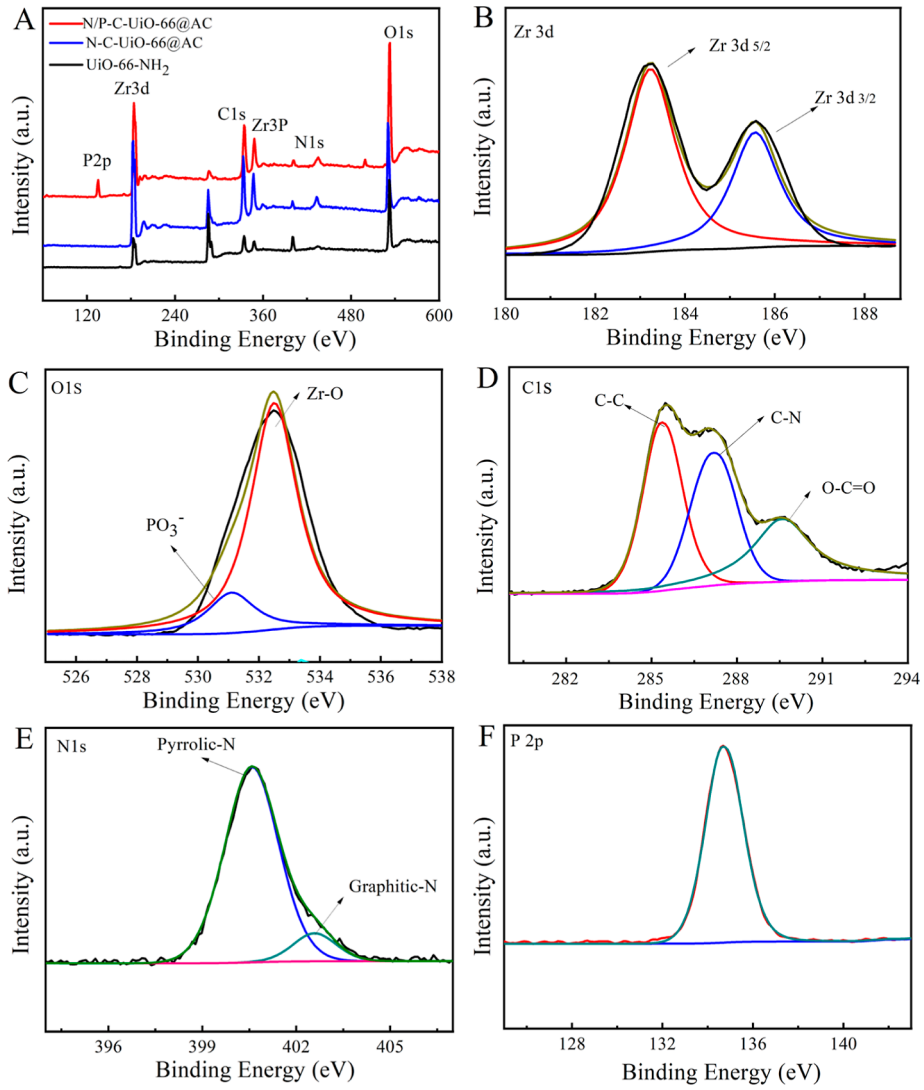

Figure 5. (A) XPS spectra of N/P-C-UiO-66@AC; (B) Zr 3d high-resolution XPS spectra; (C) O 1s high-resolution XPS spectra; (D) C 1s high-resolution XPS spectra; (E) N 1s high-resolution XPS spectra; and (F) P 2p high-resolution XPS spectra.

the GCD curves of these samples exhibit symmetric triangular shapes in the −1 to 0.2 V potential window. The discharge time of the UiO-66-NH_2 and UiO-66-PO_3 electrodes is significantly shorter compared to the carbonized samples, indicating that the energy storage performance of UiO-66-NH_2 and UiO-66-PO_3 electrodes is relatively poor. Moreover, compared with the N-C-UiO-66@AC electrode, the N/P-C-UiO-66@AC electrode has a longer discharge time and a higher specific capacitance at a current density of 1.0 A/g. This is because N/P-C-UiO-66@AC provides more electrochemically active sites for the reaction and improves the ion transport efficiency. This further confirms that doping both N and P atoms can improve the electrochemical performance of the electrode material, thereby increasing the storage capacity. Coulombic efficiency refers to the ratio of the discharge capacity and charge capacity and is an important metric to evaluate the reversibility of the SC.[25] The Coulombic efficiencies of N-C-UiO-66@AC and N/P-C-UiO-66@AC are 95.9 and 58.7%, respectively. The above results indicate that N-C-UiO-66@AC has better electrochemical reversibility than N/P-C-UiO-66@AC.

Figure 6C shows the variation of the specific capacitance of various electrode materials. The UiO-66-NH_2 and UiO-66-PO_3 electrodes exhibited a negligible specific capacitance, while N-C-UiO-66@AC and N/P-C-UiO-66@AC showed significantly higher specific capacitance. This clearly demonstrates the effectiveness of the carbonization treatment in enhancing the energy storage performance of UiO-66 materials. Furthermore, compared with the N-C-UiO-66@AC electrode, the N/P-C-UiO-66@AC electrode exhibits a smaller change in the specific capacitance and a better rate performance. Due to the low-energy storage performance of the UiO-66-NH_2 and UiO-66-PO_3, they are not suitable as energy storage materials. Therefore, we tested the *CV* curves of only N-C-UiO-66@AC and N/P-C-UiO-66@AC at a scan rate of 100 mV/s. As seen from Figure 6D, all the *CV* curves have distinct redox peaks in the range of 0.2−0.5 V, which demonstrates that the ZrO_2 formed by high-temperature carbonization of UiO-66 provides a large amount of pseudocapacitance.[30]

Figure 6E shows the GCD curves of N/P-C-UiO-66@AC at current densities ranging from 1.0 to 10 A/g. It can be seen from the figure that the GCD curve still maintains a symmetric

https://doi.org/10.1021/acsomega.3c05500
ACS Omega 2023, 8, 44689−44697

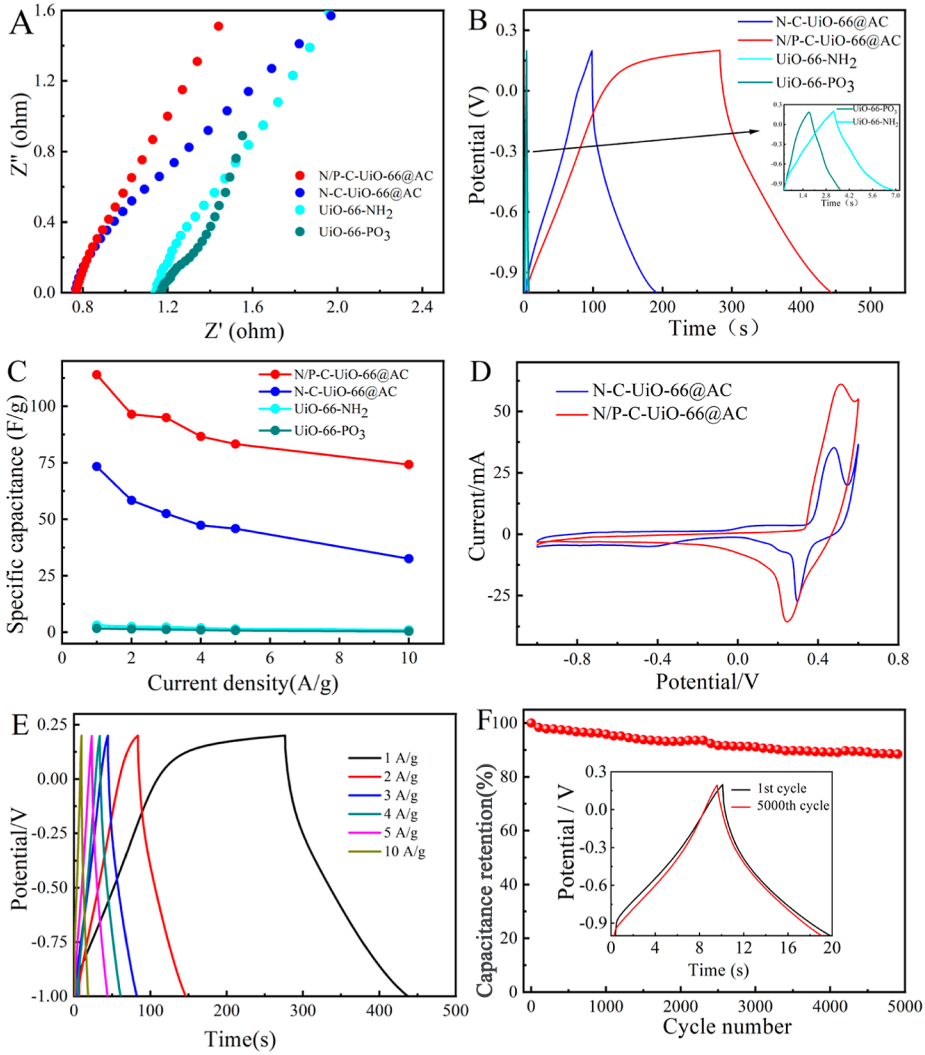

Figure 6. Three-electrode electrochemical tests of different samples: (A) Nyquist diagram; (B) GCD curves at a current density of 1 A/g; (C) specific capacitance at various current densities of 1.0−10 A/g; (D) *CV* curves of N-C-UiO-66@AC and N/P-C-UiO-66@AC at 100 mV/s; (E) GCD curves of N/P-C-UiO-66@AC at different current densities of 1.0−10 A/g; and (F) reusability performance of the N/P-C-UiO-66@AC electrode.

triangular shape as the current density increases. When the current density increases to 10 A/g, ions do not have enough time to diffuse into all of the pore structures of the electrode material, leading to a decrease in capacitance. This indicates that the N/P-C-UiO-66@AC electrode material has a high charge−discharge reversibility and good rate performance. The cycling stability of the material plays a crucial role in their practical applications.[31−33] As shown in Figure 6F, GCD tests were carried out at a current density of 10 A/g to study the cycling stability of N/P-C-UiO-66@AC. After 5000 cycles of repeated charge and discharge, the specific capacitance retention rate was 88.5%. The inset in Figure 6F shows a comparison between the GCD curves before and after 5000 cycles at a current density of 10 A/g. From the graph, it can be seen that there is little change in charge and discharge time before and after cycling, indicating that the prepared N/P-C-UiO-66@AC electrode has good cycling stability and energy storage capacity.

Table 1 summarizes the comparison of the electrochemical performance of N/P-C-UiO-66@AC and other reported carbon-based nanocomposite electrode materials. From the table, it can be seen that the N/P-C-UiO-66@AC prepared in this experiment has the best electrochemical performance, which can be attributed to several reasons: (i) ZrO_2 formed by high-temperature calcination can effectively provide a large amount of pseudocapacitance; (ii) the high-temperature carbonization of UiO-66 and the introduction of AC have improved the conductivity of the material; and (iii) simultaneous doping of nitrogen (N) and phosphorus (P)

Table 1. Comparison of the Electrochemical Properties of Carbon-Based Nanocomposites

electrode material	current density	specific capacitance	references
C-UiO-66-AT[a]	1.0 A/g	117 F/g	17
C-UiO-66	20 mV/s	32.7 F/g	34
PANI/ZrO_2	0.2 A/g	127 F/g	35
C/Zn-MOF	0.5 A/g	138 F/g	36
NiO film/ITO[b]	1.0 mA/cm^2	2.08 F/cm^2	37
N/P-C-UiO-66@AC	1.0 A/g	140 F/g	this work

[a]UiO-66 subjected to carbonization and acid treatment. [b]Indium tin oxide.

https://doi.org/10.1021/acsomega.3c05500
ACS Omega 2023, 8, 44689−44697

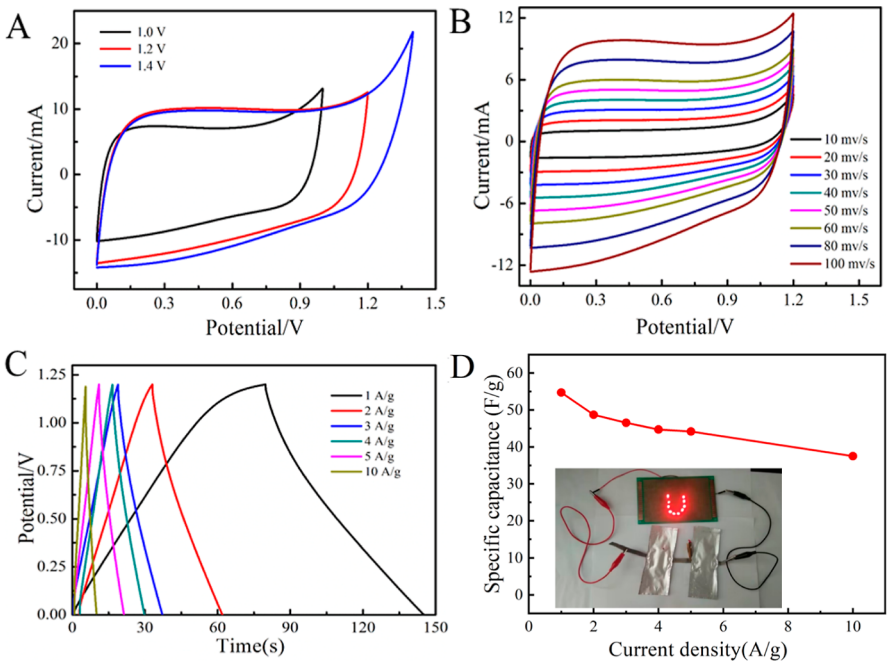

Figure 7. Electrochemical performance of the N/P-C-UiO-66@AC//N/P-C-UiO-66@AC symmetric supercapacitor in a 6 M KOH electrolyte: (A) *CV* curves at different voltage ranges at the scanning rate of 100 mV/s; (B) *CV* curves at different scanning rates of 10−100 mV/s; (C) GCD curves at different current densities of 1.0−10 A/g; and (D) specific capacitance curve of N/P-C-UiO-66@AC//N/P-C-UiO-66@AC symmetric supercapacitors. Inset is a photograph of LED lights lit with symmetric supercapacitors.

atoms can provide more active sites for the Faraday reaction and increase the efficiency of ion transport.

3.3. Performance of the Symmetric Supercapacitor. In order to further evaluate the practical application value of the N/P-C-UiO-66@AC electrode, a symmetrical SC was assembled by using two identical N/P-C-UiO-66@AC electrodes in a solution containing 6.0 M KOH. Figure 7A shows the *CV* curve of N/P-C-UiO-66@AC//N/P-C-UiO-66@AC at different potential windows (1.0−1.4 V). It can be observed from the figure that the curve remains nearly rectangular at the voltage window of 0−1.2 V, and the anodic current does not increase significantly. However, when the voltage window reaches 1.4 V, the anodic current increases rapidly due to the electrolysis reaction of water. This indicates that the SCs have good electrochemical reversibility and capacitance performance at a voltage of 1.2 V. Therefore, the performance of N/P-C-UiO-66@AC//N/P-C-UiO-66@AC was tested in the voltage window of 0−1.2 V. Figure 7B shows its CV curve at different scan rates (10−100 mV/s). As seen, even at a high scan rate of 100 mV/s, the *CV* curve remains rectangular, indicating that N/P-C-UiO-66@AC//N/P-C-UiO-66@AC has good electrochemical reversibility.

To further study the rate performance of N/P-C-UiO-66@AC//N/P-C-UiO-66@AC, GCD tests were conducted. Figure 7C shows the GCD curves of the SC tested at current densities of 1.0−10 A/g. It can be observed from the figure that all GCD curves are isosceles triangles, indicating that N/P-C-UiO-66@AC//N/P-C-UiO-66@AC has a low internal resistance. Figure 7D shows the specific capacitance of the capacitor obtained based on the GCD curve at current densities of 1.0−10 A/g. The specific capacitance is 55 F/g at a low current density of 1.0 A/g and 38 F/g (retaining 69%) at a high current density of 10 A/g, indicating that the SC has high specific capacitance and excellent rate performance. The insert in Figure 7D shows that N/P-C-UiO-66@AC//N/P-C-UiO-66@AC can light up an LED, indicating that the SC has certain practical application value.

Figure 8 is the Ragone plot of the N/P-C-UiO-66@AC//N/P-C-UiO-66@AC symmetric SC. As seen, the energy density

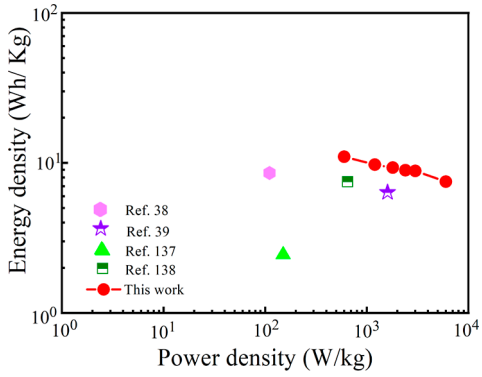

Figure 8. Ragone diagram of N/P-C-UiO-66@AC//N/P-C-UiO-66@AC symmetric supercapacitors and other MOF-based symmetric supercapacitors reported in the literature.

of the N/P-C-UiO-66@AC//N/P-C-UiO-66@AC is higher than those of the previously reported electrode materials for SCs.[38−41] When the power density is 600 W/kg, the energy density of N/P-C-UiO-66@AC//N/P-C-UiO-66@AC can reach 11.0 W h/kg. Even at a high power density of 6000 W/kg, its energy density could still be maintained at 7.5 W h/kg.

4. CONCLUSIONS

In this work, a simple method was used to successfully prepare N/P-C-UiO-66@AC composite materials. The electrical conductivity and capacitance of UiO-66 were improved by using carbonization and the addition of AC. In addition, the

https://doi.org/10.1021/acsomega.3c05500
ACS Omega 2023, 8, 44689−44697

introduction of nitrogen (N) and phosphorus (P) further provides more active sites for Faradaic reactions and increases the efficiency of the ion transport. The electrochemical test results showed that the specific capacitance of the N/P-C-UiO-66@AC electrode could reach up to 140 F/g at a current density of 1.0 A/g. Furthermore, after 5000 cycles of charge and discharge at a current density of 10 A/g, the capacitance retention rate remained at 88.5%. These test results indicated that the SCs assembled with this electrode material had good storage capacity, excellent cycling stability, and an outstanding rate performance. The N/P-C-UiO-66@AC//N/P-C-UiO-66@AC symmetric SC assembled with this electrode material had an energy density of 11.0 W h/kg and a power density of 600 W/kg. Even at a high power density of 6000 W/kg, its energy density could still be maintained at 7.5 W h/kg. Therefore, this method can provide a certain reference for the development of high-performance SCs in the future.

AUTHOR INFORMATION

Corresponding Authors

Rong Chen − *Jiangxi Province Key Laboratory of Polymer Micro/Nano Manufacturing and Devices, East China University of Technology, Nanchang 330013 Jiangxi, China*; Email: 200660009@ecut.edu.cn

Tianxiang Jin − *Jiangxi Province Key Laboratory of Polymer Micro/Nano Manufacturing and Devices, East China University of Technology, Nanchang 330013 Jiangxi, China*; orcid.org/0000-0001-5950-6792; Email: 201660027@ecut.edu.cn

Authors

Chunyan Wang − *Jiangxi Province Key Laboratory of Polymer Micro/Nano Manufacturing and Devices, East China University of Technology, Nanchang 330013 Jiangxi, China*

Jingwei Su − *Jiangxi Province Key Laboratory of Polymer Micro/Nano Manufacturing and Devices, East China University of Technology, Nanchang 330013 Jiangxi, China*

Haiyan Lan − *Jiangxi Province Key Laboratory of Polymer Micro/Nano Manufacturing and Devices, East China University of Technology, Nanchang 330013 Jiangxi, China*

Chongshi Wang − *College of Engineering, Department of Civil, Architectural & Environmental Engineering, Drexel University, Philadelphia, Pennsylvania 19104, United States*

Yi Zeng − *Jiangxi Province Key Laboratory of Polymer Micro/Nano Manufacturing and Devices, East China University of Technology, Nanchang 330013 Jiangxi, China*

Complete contact information is available at: https://pubs.acs.org/10.1021/acsomega.3c05500

Author Contributions

§C.W. and J.S. contributed equally to this work and share first authorship.

Notes

The authors declare no competing financial interest.

ACKNOWLEDGMENTS

The authors are grateful for the financial support of the Opening Project of Jiangxi Province Key Laboratory of Polymer Micro/Nano Manufacturing and Devices (PMND202201), the Natural Science Foundation of Jiangxi Province (20202BABL213011), and College Students' Innovative Entrepreneurial Training Plan Program (202210405016).

REFERENCES

(1) Raza, W.; Ali, F.; Raza, N.; Luo, Y.; Kim, K.-H.; Yang, J.; Kumar, S.; Mehmood, A.; Kwon, E. E. Recent advancements in supercapacitor technology. *Nano Energy* **2018**, *52*, 441−473.

(2) Chen, J.; Lin, C.; Zhang, M.; Jin, T.; Qian, Y. Constructing Nitrogen, Selenium Co-Doped Graphene Aerogel Electrode Materials for Synergistically Enhanced Capacitive Performance. *ChemElectroChem* **2020**, *7* (15), 3311−3318.

(3) Ren, G.; Li, Y.; Chen, Q.; Qian, Y.; Zheng, J.; Zhu, Y.; Teng, C. Sepia-derived N, P co-doped porous carbon spheres as oxygen reduction reaction electrocatalyst and supercapacitor. *ACS Sustainable Chem. Eng.* **2018**, *6* (12), 16032−16038.

(4) Ng, W.; Yang, Y.; van der Veen, K.; Rothenberg, G.; Yan, N. Enhancing the performance of 3D porous N-doped carbon in oxygen reduction reaction and supercapacitor via boosting the meso-macropore interconnectivity using the "exsolved" dual-template. *Carbon* **2018**, *129*, 293−300.

(5) Zhu, T.; Ding, J.; Shao, Q.; Qian, Y.; Huang, X. P, Se-Codoped MoS2 Nanosheets as Accelerated Electrocatalysts for Hydrogen Evolution. *ChemCatChem* **2019**, *11* (2), 689−692.

(6) Yue, D.; Yang, J.-x.; Sun, B.; Shi, K.; Zhu, H.; Li, X.-k. Preparation and electrochemical performance of the N-doped hollow pitch-based activated carbon fibers as supercapacitor electrodes. *Carbon* **2020**, *167*, 931.

(7) Hulicova-Jurcakova, D.; Puziy, A. M.; Poddubnaya, O. I.; Suárez-García, F.; Tascón, J. M. D.; Lu, G. Q. Highly stable performance of supercapacitors from phosphorus-enriched carbons. *J. Am. Chem. Soc.* **2009**, *131* (14), 5026−5027.

(8) Wen, Y.; Rufford, T. E.; Hulicova-Jurcakova, D.; Wang, L. Nitrogen and Phosphorous Co-Doped Graphene Monolith for Supercapacitors. *ChemSusChem* **2016**, *9* (5), 513−520.

(9) Zhou, H. C. J.; Kitagawa, S. Metal-organic frameworks (MOFs). *Chem. Soc. Rev.* **2014**, *43* (16), 5415−5418.

(10) Li, W.; Guo, X.; Geng, P.; Du, M.; Jing, Q.; Chen, X.; Zhang, G.; Li, H.; Xu, Q.; Braunstein, P.; et al. Rational design and general synthesis of multimetallic metal-organic framework nano-octahedra for enhanced Li-S battery. *Adv. Mater.* **2021**, *33* (45), 2105163.

(11) Geng, P.; Wang, L.; Du, M.; Bai, Y.; Li, W.; Liu, Y.; Chen, S.; Braunstein, P.; Xu, Q.; Pang, H. MIL-96-Al for Li-S batteries: shape or size? *Adv. Mater.* **2022**, *34* (4), 2107836.

(12) Zheng, S.; Sun, Y.; Xue, H.; Braunstein, P.; Huang, W.; Pang, H. Dual-ligand and hard-soft-acid-base strategies to optimize metal-organic framework nanocrystals for stable electrochemical cycling performance. *Natl. Sci. Rev.* **2022**, *9* (7), nwab197.

(13) Tan, Y.; Zhang, W.; Gao, Y.; Wu, J.; Tang, B. Facile synthesis and supercapacitive properties of Zr-metal organic frameworks (UiO-66). *RSC Adv.* **2015**, *5* (23), 17601−17605.

(14) Bhadu, G. R.; Parmar, B.; Patel, P.; Paul, A.; Chaudhari, J. C.; Srivastava, D. N.; Suresh, E. Co@N-doped carbon nanomaterial derived by simple pyrolysis of mixed-ligand MOF as an active and stable oxygen evolution electrocatalyst. *Appl. Surf. Sci.* **2020**, *529*, 147081.

(15) Du, M.; Geng, P.; Pei, C.; Jiang, X.; Shan, Y.; Hu, W.; Ni, L.; Pang, H. High-Entropy Prussian Blue Analogues and Their Oxide Family as Sulfur Hosts for Lithium-Sulfur Batteries. *Angew. Chem., Int. Ed.* **2022**, *61* (41), No. e202209350.

(16) Li, Z.; Liu, X.; Wang, L.; Bu, F.; Wei, J.; Pan, D.; Wu, M. Hierarchical 3D All-Carbon Composite Structure Modified with N-Doped Graphene Quantum Dots for High-Performance Flexible Supercapacitors. *Small* **2018**, *14* (39), 1801498.

(17) Sung, Y.-S.; Lin, L.-Y. Improving energy storage ability of Universitetet i Oslo-66 as active material of supercapacitor using carbonization and acid treatment. *J. Energy Storage* **2021**, *37*, 102480.

(18) Guo, Y.; Jin, H.; Qi, Z.; Hu, Z.; Ji, H.; Wan, L. J. Carbonized-MOF as a Sulfur Host for Aluminum-Sulfur Batteries with Enhanced Capacity and Cycling Life. *Adv. Funct. Mater.* **2019**, *29* (7), 1807676.

(19) Li, G.; Qi, X.; Wu, J.; Xu, L.; Wan, X.; Liu, Y.; Chen, Y.; Li, Q. Ultrasensitive, label-free voltammetric determination of norfloxacin based on molecularly imprinted polymers and Au nanoparticle-functionalized black phosphorus nanosheet nanocomposite. *J. Hazard. Mater.* **2022**, *436*, 129107.
(20) Wu, Y.; Xiao, Y.; Yuan, H.; Zhang, Z.; Shi, S.; Wei, R.; Gao, L.; Xiao, G. Imidazolium ionic liquid functionalized UiO-66-NH2 as highly efficient catalysts for chemical fixation of CO2 into cyclic carbonates. *Microporous Mesoporous Mater.* **2021**, *310*, 110578.
(21) Dorneles de Mello, M.; Kumar, G.; Tabassum, T.; Jain, S. K.; Chen, T. H.; Caratzoulas, S.; Li, X.; Vlachos, D. G.; Han, S. I.; Scott, S. L.; et al. Phosphonate-Modified UiO-66 Brønsted Acid Catalyst and Its Use in Dehydra-Decyclization of 2-Methyltetrahydrofuran to Pentadienes. *Angew. Chem., Int. Ed.* **2020**, *59* (32), 13260−13266.
(22) Zhong, W.; Zou, J.; Yu, Q.; Gao, Y.; Qu, F.; Liu, S.; Zhou, H.; Lu, L. Ultrasensitive indirect electrochemical sensing of thiabendazole in fruit and water by the anodic stripping voltammetry of Cu2+ with hierarchical Ti3C2Tx-TiO2 for signal amplification. *Food Chem.* **2023**, *402*, 134379.
(23) Fakhri, A.; Behrouz, S.; Tyagi, I.; Agarwal, S.; Gupta, V. K. Synthesis and characterization of ZrO2 and carbon-doped ZrO2 nanoparticles for photocatalytic application. *J. Mol. Liq.* **2016**, *216*, 342−346.
(24) Wang, X.; Hong, H.; Yang, S.; Bai, S.; Yang, R.; Jin, X.; Zhi, C.; Wang, B. A UiO-66-NH 2 MOF derived N doped porous carbon and ZrO 2 composite cathode for zinc-ion hybrid supercapacitors. *Inorg. Chem. Front.* **2023**, *10* (7), 2115−2124.
(25) Chen, C.; Deng, H.; Wang, C.; Luo, W.; Huang, D.; Jin, T. Petal-like CoMoO4 clusters grown on carbon cloth as a binder-free electrode for supercapacitor application. *ACS Omega* **2021**, *6* (30), 19616−19622.
(26) Li, G.; Liu, Y.; Chen, Y.; Li, M.; Song, J.; Li, K.; Zhang, Y.; Hu, L.; Qi, X.; Wan, X.; et al. Polyvinyl alcohol/polyacrylamide double-network hydrogel-based semi-dry electrodes for robust electroencephalography recording at hairy scalp for noninvasive brain-computer interfaces. *J. Neural Eng.* **2023**, *20* (2), 026017.
(27) Li, G.; Qi, X.; Zhang, G.; Wang, S.; Li, K.; Wu, J.; Wan, X.; Liu, Y.; Li, Q. Low-cost voltammetric sensors for robust determination of toxic Cd(II) and Pb(II) in environment and food based on shuttle-like α-Fe2O3 nanoparticles decorated β-Bi2O3 microspheres. *Microchem. J.* **2022**, *179*, 107515.
(28) Zhu, M.; Shao, Q.; Pi, Y.; Guo, J.; Huang, B.; Qian, Y.; Huang, X. Ultrathin Vein-Like Iridium-Tin Nanowires with Abundant Oxidized Tin as High-Performance Ethanol Oxidation Electrocatalysts. *Small* **2017**, *13* (36), 1701295.
(29) Li, G.; Wu, J.; Qi, X.; Wan, X.; Liu, Y.; Chen, Y.; Xu, L. Molecularly imprinted polypyrrole film-coated poly(3,4-ethylenedioxythiophene):polystyrene sulfonate-functionalized black phosphorene for the selective and robust detection of norfloxacin. *Mater. Today Chem.* **2022**, *26*, 101043.
(30) Li, G.; Ren, M.; Zhou, H. Observably boosted electrochemical performances of roughened graphite sheet/polyaniline electrodes for use in flexible supercapacitors. *Surf. Interfaces* **2022**, *30*, 101874.
(31) Zhu, S.-X.; Li, Z.-M.; Gong, W.-Q.; Gao, Z.-T.; Guan, H.; Sun, M.-S.; Zhou, Y.; Tao, D.-J. Equimolar CO Capture by Cuprous-Based Quaternary Deep Eutectic Solvents. *Ind. Eng. Chem. Res.* **2023**, *62* (6), 2937−2943.
(32) Tao, D.-J.; An, X.-C.; Gao, Z.-T.; Li, Z.-M.; Zhou, Y. Cuprous-based composite ionic liquids for the selective absorption of CO: Experimental study and thermodynamic analysis. *AIChE J.* **2022**, *68* (5), No. e17631.
(33) Tao, D.-J.; Qu, F.; Li, Z.-M.; Zhou, Y. Promoted absorption of CO at high temperature by cuprous-based ternary deep eutectic solvents. *AIChE J.* **2021**, *67* (2), No. e17106.
(34) Huo, X.; Jing, Z.; Wang, H.; Chang, N. Sodium dodecyl sulfate/C-UIO-66 regulation of nanofiltration membrane with pleated and thin polyamide layer structure. *Desalination* **2022**, *538*, 115927.
(35) Sinha, S.; Singh, W. I.; Nongthombam, S.; Devi, N. A.; Laha, S.; Swain, B. S.; Swain, B. P. Optical properties, electrochemical analysis and corrosion resistance studies of polyaniline/reduced graphene Oxide/ZrO2 for supercapacitor application. *J. Phys. Chem. Solids* **2022**, *161*, 110478.
(36) Yue, M. L.; Yu, C. Y.; Duan, H. H.; Yang, B. L.; Meng, X. X.; Li, Z. X. Six Isomorphous Window-Beam MOFs: Explore the Effects of Metal Ions on MOF-Derived Carbon for Supercapacitors. *Chem.—Eur. J.* **2018**, *24* (60), 16160−16169.
(37) Emam-Ismail, M.; El-Hagary, M.; El-Sherif, H.; El-Naggar, A.; El-Nahass, M. Spectroscopic ellipsometry and morphological studies of nanocrystalline NiO and NiO/ITO thin films deposited by e-beams technique. *Opt. Mater.* **2021**, *112*, 110763.
(38) Chowdhury, T. S.; Grebel, H. Supercapacitors with electrical gates. *Electrochim. Acta* **2019**, *307*, 459−464.
(39) Fukuhara, M.; Kuroda, T.; Hasegawa, F. Amorphous titanium-oxide supercapacitors. *Sci. Rep.* **2016**, *6* (1), 35870.
(40) Marriam, I.; Wang, Y.; Tebyetekerwa, M. Polyindole batteries and supercapacitors. *Energy Storage Mater.* **2020**, *33*, 336−359.
(41) Vijayakumar, M.; Bharathi Sankar, A.; Sri Rohita, D.; Rao, T. N.; Karthik, M. Conversion of biomass waste into high performance supercapacitor electrodes for real-time supercapacitor applications. *ACS Sustainable Chem. Eng.* **2019**, *7* (20), 17175−17185.

https://doi.org/10.1021/acsomega.3c05500
ACS Omega 2023, 8, 44689−44697